Physical-Layer-Aware Performance Evaluation of SDM Networks Based on SMF Bundles, MCFs, and FMFs

Behnam Shariati, Antonia Mastropaolo, Nikolaos-Panteleimon Diamantopoulos, José Manuel Rivas-Moscoso, Dimitrios Klonidis, and Ioannis Tomkos

***Abstract*—In this work, we compare the performance of several space division multiplexing (SDM) network realizations utilizing different types of transmission media. In this regard, we first present a tool developed for the estimation of signal quality degradation in SDM-based optical networks. The tool supports SDM networks utilizing few-mode fibers (FMFs) and multicore fibers (MCFs), as well as bundles of single-mode fibers (BuSMFs), and provides an accurate quality of transmission (QoT) estimation allowing the network operators and designers to take into account physical layer impairments while performing network planning analysis. Considering the proposed QoT tool, we present extensive simulation results comparing the performance of FMFs, MCFs, and BuSMFs in terms of maximum achievable optical transparent reach in a multispan point-to-point scenario, where the impact of amplifier span length, channel spacing, and number of co-propagating spectral channels is studied. These results are used to perform physical-layer-aware SDM network planning analysis following the LOGON approach, which allows us to evaluate the impact of reach-limited transmission along different types of fibers in a networking scenario for different sizes of an optical network topology. The results of this study compare different SDM network realizations in terms of average spectrum utilization and the number of in-operation transceivers operating over different modulation formats showcasing the benefits and drawbacks of SDM networks relying on different transmission media.**

***Index Terms*—Optical networks; Quality of transmission estimator; Space division multiplexing.**

I. Introduction

Spatially-spectrally flexible optical networking, based on space division multiplexing (SDM) technology and elastic optical networking, is anticipated to be the solution addressing the "capacity crunch" with a reduced cost per bit delivered to end-users [1–4]. The cost reduction could be achieved by introducing some levels of component sharing and integration [5]. To this extent, significant research efforts have focused on the development of few-mode fibers (FMFs) and multicore fibers (MCFs), which are favorable "integrated fiber" options for SDM networks [6]. Bundles of single-mode fibers (BuSMFs) is another SDM transmission medium that is considered as a cost-effective option for early SDM implementations, since it aggregates fibers already deployed on the ground. The choice of one of these transmission media is a key factor in determining the required architecture and properties of the optical switches at the nodes of an SDM-based network. In this regard, different switching strategies for SDM networks are identified [7,8], namely independent switching (Ind-Sw), fractional joint switching (FrJ-Sw), and joint switching (J-Sw), in order of decreasing flexibility and increasing hardware efficiency and spatial integration. Ind-Sw handles every spatial dimension independently, whereas J-Sw treats all of them as a single entity. J-Sw is compatible with any type of SDM transmission medium, whereas FrJ-Sw and Ind-Sw are fiber-dependent [9]. Fiber types and switching nodes are two main technology areas determining the channel allocation strategies in SDM networks, due to the physical impairments introduced and the routing constraints imposed. Therefore, several channel allocation policies are identified for SDM networks, which can generally be categorized into two groups [2], namely, (a) spectral superchannel (Sp-Ch) allocation policy, in which demands spread over a contiguous portion of spectrum in a single spatial dimension, and (b) spatial Sp-Ch allocation policy, in which demands spread across a number or all of the spatial dimensions over a given spectral slice. These channel allocation strategies are compared in Ref. [10]. Additionally, the performance of SDM switching paradigms is thoroughly investigated in Refs. [8–12]. However, there has been a limited effort in evaluating the impact of physical layer impairments introduced by SDM fibers on the performance of SDM networks.

The physical impairments introduced by SDM fibers are classified into two groups, namely, (i) intramodal impairments and (ii) inter-modal impairments. All transmission media are affected by intramodal linear and nonlinear

Manuscript received March 16, 2018; revised May 24, 2018; accepted June 25, 2018; published July 26, 2018 (Doc. ID 326129).

B. Shariati (e-mail: b.shariati@ait.gr) was with Athens Information Technology (AIT), Athens, Greece. He is now with Universitat Politécnica de Catalunya (UPC), Barcelona, Spain.

A. Mastropaolo was with Athens Information Technology (AIT), Athens, Greece. She is now with the Polytechnic University of Turin, Turin, Italy.

N.-P. Diamantopoulos was with Athens Information Technology (AIT), Athens, Greece. He is now with NTT Device Technology Laboratories, NTT Corporation, Kanagawa, Japan.

J. M. Rivas-Moscoso was with Athens Information Technology (AIT), Athens, Greece.

D. Klonidis and I. Tomkos are with Athens Information Technology (AIT), Athens, Greece.

https://doi.org/10.1364/JOCN.10.000712

 Journal © 2018 Optical Society of America

impairments. Furthermore, MCFs and FMFs also present inter-modal impairments, viz., MCFs are affected by inter-core crosstalk (XT) and FMFs are impacted by mode coupling, differential group delay (DGD), mode-dependent losses (MDLs), and inter-modal nonlinearities. Digital signal processing (DSP) techniques, including multi-input multi-output (MIMO) processing, have been developed in order to compensate for the abovementioned inter-modal linear impairments [13], although they result in a significant increase in the power consumption of the transceiver [14]. Nonlinear impairments, nonetheless, are unlikely to be compensated for with the current DSP modules and, therefore, could result in significant performance degradation.

Having said that, the design and operation of optical networks should take into account transmission impairments for the assignment of appropriate spectral and spatial network resources while establishing the lightpaths. The established lightpaths must have a guaranteed quality of transmission (QoT) ensuring adequate transmission performance over the lightpath length. Simple scaling rules have been developed for estimating signal degradation for spectrally flexible optical networks, based on SMFs, in order to provide an accurate QoT estimation for network operators and designers [15]. However, limited efforts have been made for SDM networks, which are based on alternative transmission media. In Ref. [16], for weakly coupled MCFs (WC-MCFs), a formulation has been provided for the intercore XT in the resource allocation problem. The authors of Ref. [17] expanded the previous work by taking into account both intracore and inter-core impairments together. In Ref. [18], for the case of FMFs, the inter-modal XT is modeled by deriving a normalized value of the modal XT from an existing experiment. In addition, in Ref. [19], an analytical model is proposed for evaluating the impact of MDLs on the provisioning capacity of an FMF-based network. However, none of these works present a single tool accounting for all intra- and inter-modal linear and nonlinear impairments induced by different SDM fibers.

In this paper, we present a QoT estimator developed particularly for SDM networks, which accounts for physical impairments (i.e., intra- and inter-modal linear and nonlinear impairments) of WC-MCFs, FMFs, and also BuSMFs. The target of our paper is to use existing (analytical) models to develop a QoT estimator. Since the QoT estimator requires very fast processing, numerical models had to be avoided. This tool allows for estimating the signal QoT, evaluating the impact of the impairments on the system performance [e.g., optical signal-to-noise ratio (OSNR), optical reach, etc.], and providing a flexible platform to test and compare different scenarios. The tool is then used for physical-layer-aware SDM network performance evaluations exploiting the LOGO approach [15]. The rest of the paper is organized as follows: the derivation of the analytical model enabling the realization of the QoT estimator, the QoT estimator, its principle of operation, and the corresponding simulation results are discussed in Section II. In Section III, the benefits of utilizing the QoT estimator for SDM network planning practices are demonstrated by presenting a set of network-wide performance evaluations comparing various SDM network implementations. Finally, concluding remarks are presented in Section V.

II. Quality of Transmission Estimator

We have developed a QoT estimator for SDM networks that calculates the performance of coherent multilevel phase-modulated signals when propagated over an optical uncompensated SDM link (i.e., FMFs, MCFs, and BuSMFs) composed of several amplified spans. In this work, we consider FMFs with M linearly polarized (LP) spatial modes. Hence, the total mode count including the polarizations is $2M$. The tool supports SDM networks based on both fixed-grid wavelength division multiplexing (WDM) and gridless multicarrier multiplexing schemes exploiting Nyquist WDM and orthogonal frequency division multiplexing. The estimator predicts the QoT of a lightpath to be established in a multispan point-to-point transmission scenario. Additionally, it is capable of predicting the QoT of new lightpaths to be established in a network, as well as their impact on the existing lightpaths.

The QoT estimation mechanism uses information about the network topology, link characteristics, signal types (Baud rate and modulation format), and lightpaths currently established in the network (i.e., occupied spectral slots on each spatial mode). The estimated QoT is expressed in OSNR per spatial channel and can be translated to Q-factor, bit error rate (BER), error vector magnitude, or optical reach value (in kilometers).

In this work, we aim at developing a QoT estimator by using the existing analytical models for each SDM fiber. The OSNR for each SDM fiber type is determined based on analytical models, whose accuracy is verified through experimental evaluations [15,20], taking into account impairments that are unlikely to be compensated for by DSP at the receiver. So, it is important to have in mind that the analytical models described in the next sections are already available models with demonstrated accuracy through experimental evaluations. The computational complexity of the models considered is low enough to allow the use of the QoT estimator for network planning and operation practices.

III. Analytical Models

A. Analytical Model for FMFs

The closed-form solution used in the QoT estimator for the FMF transmission is the one presented in Refs. [20,21] and was derived from the Manakov equations for FMFs [22]. A similar approach has also been followed in Ref. [23]. The model is derived assuming a weak-coupling regime; this means the coupling between spatial modes is small or negligible, but the coupling between polarizations is considered strong. As shown in Refs. [21,22,24], the strong-coupling regime is expected to reduce the modal dispersion and nonlinear effects, and thus could be used to design optimized fibers where the impact of nonlinear

impairments is reduced [25]. Here, however, working in the weak-coupling regime serves well the current scope of this paper, as it can be considered a worst-case scenario for the nonlinear impairments [22]. Yet, additional investigations for the strong-coupling regime are important and we leave these studies for future works. The Manakov equations can be written in a simplified form [22]:

$$\frac{\partial \vec{A}^{(p)}}{\partial} + \frac{\alpha}{2}\vec{A}^{(p)} - i\left(\beta_0^{(p)} - \beta_0^{(1)}\right)\vec{A}^{(p)} + \left(\beta_1^{(p)} - \beta_1^{(1)}\right)\frac{\partial \vec{A}^{(p)}}{\partial t} + i\frac{\beta_2^{(p)}}{2}\frac{\partial^2 \vec{A}^{(p)}}{\partial t^2} = i\left(\tilde{\gamma}^{(pppp)}\left|\vec{A}^{(p)}\right|^2 + \sum_{m\neq p}\tilde{\gamma}^{(mmpp)}\left|\vec{A}^{(m)}\right|^2\right)\vec{A}^{(p)}, \tag{1}$$

where $\vec{A}^{(p)}(z,t) = [A_x^{(p)}(z,t), A_y^{(p)}(z,t)]^T$ is the slowly varying envelope of the pth spatial mode accounting for both x and y polarizations, propagating toward z direction, in a moving frame referenced to the group velocity $v_g^{(1)}$ of the first spatial mode.

Here, α is the attenuation coefficient and $\beta_0^{(u)}$, $\beta_1^{(u)}$, and $\beta_2^{(u)}$ are the first three terms of the Taylor expansion of the propagation constant for spatial mode p, indicating, respectively, the mode's phase constant, the inverse group velocity, and the group velocity dispersion (GVD).

The nonlinear coefficients are defined as [26]:

$$\tilde{\gamma}^{(pppp)} = \kappa^{(pp)}\gamma^{(pppp)} = \frac{4}{3}\frac{2M}{2M-1}\frac{\omega_0 n_2}{cA_{\text{eff}}^{(pppp)}}, \quad \text{(intra-modal)}, \tag{2}$$

$$\tilde{\gamma}^{(mmpp)} = \kappa^{(mp)}\gamma^{(mmpp)} = \frac{4}{3}\frac{\omega_0 n_2}{cA_{\text{eff}}^{(mmpp)}}, \quad \text{(inter-modal)}, \tag{3}$$

where c denotes the speed of light in vacuum, ω_0 is the angular frequency, n_2 is the nonlinear refractive index, M is the number of spatial modes in the FMF, and $\kappa^{(pp)}$ and $\kappa^{(mp)}$ are the intra- and inter-modal averaging factors, given by $\frac{4}{3}\frac{2M}{2M-1}$ and $\frac{4}{3}$, respectively [21]. $A_{\text{eff}}^{(pppp)}$ and $A_{\text{eff}}^{(mmpp)}$ are, respectively, the intramodal and inter-modal effective areas, as defined in Ref. [23].

For the sake of clarity, in the rest of the equations presented, superscripts define spatial mode indexing and subscripts define wavelength indexing. The interaction of three wavelengths λ_1, λ_2, and λ_3, propagating in different spatial modes denoted, respectively, as m, n, and p, generates a nonlinear signal $E_{\lambda_4}^{(r)}$ at a frequency of $\omega_{\lambda_4} = \omega_{\lambda_1} + \omega_{\lambda_2} - \omega_{\lambda_3}$ in spatial mode r as a consequence of four-wave mixing (FWM) [20,21]:

$$E_{\lambda_4}^{(r)} = \tilde{\gamma}^{(mnpr)}E_{\lambda_1}^{(m)}E_{\lambda_2}^{(n)}E_{\lambda_3}^{(p)}\frac{1-e^{-\alpha L}e^{-j\Delta\beta_{\lambda_1\lambda_2\lambda_3\lambda_4}^{(mnpr)}L}}{j\Delta\beta_{\lambda_1\lambda_2\lambda_3\lambda_4}^{(mnpr)}L+\alpha}e^{-\alpha/2L}e^{-j\beta_{ds}L}, \tag{4}$$

where L is the span length; $\tilde{\gamma}^{(mnpr)}$ is the nonlinear coefficient for the interaction of spatial modes m, n, p, r; and $\Delta\beta_{\lambda_1\lambda_2\lambda_3\lambda_4}^{(mnpr)} = \beta_{\lambda_1}^{(m)} + \beta_{\lambda_2}^{(n)} - \beta_{\lambda_3}^{(p)} - \beta_{\lambda_4}^{(r)}$ is the phase mismatch between wavelengths λ_1, λ_2, λ_3, and λ_4, with $\beta_{\lambda_1}^{(m)}$, $\beta_{\lambda_2}^{(n)}$, $\beta_{\lambda_3}^{(p)}$, and $\beta_{\lambda_4}^{(r)}$ being the propagation constants of spatial modes m, n, p, and r at angular frequencies of ω_{λ_1}, ω_{λ_2}, ω_{λ_3}, and ω_{λ_4}, respectively.

The total nonlinear power generated by the effect of FWM for a superchannel with a total bandwidth of B can be obtained by integrating the product of the electrical field in Eq. (4) and the signal power spectral density (PSD) in each spatial mode over frequencies ω_{λ_1}, ω_{λ_2}, and ω_{λ_3}. The closed form of this integral is derived in Ref. [19] under the assumption that the spectrum signal is rectangular as in the case of Nyquist WDM. The derivation of the closed form has led to the definition of the following FWM efficiency parameter [20,21]:

$$\eta^{(mnpr)} = \frac{[\tilde{\gamma}^{(mnpr)}]^2}{2\pi\alpha|\beta_2|}\left[\ln\left(\frac{B^2+2B\Delta f^{(mnpr)}}{2f_w^2}\right) + \bar{S}\ln\left(\bar{s}\frac{B^2-2B\Delta f^{(mnpr)}}{2f_w^2}\right)\right]. \tag{5}$$

The term f_w is the walk-off bandwidth indicating the frequency range of the effectiveness of FWM nonlinearity in the presence of the dispersion defined as:

$$f_w = \sqrt{\frac{\alpha}{4\pi^2|\beta_2|}}. \tag{6}$$

The terms $\bar{S}$ and $\Delta f^{(abcd)}$ are defined, respectively, as:

$$\bar{S} = \text{sign}(B - 2\Delta f^{(mnpr)}) \tag{7}$$

and

$$\Delta f^{(mnpr)} = \frac{(\beta_1^{(m)} + \beta_1^{(n)} - \beta_1^{(p)} - \beta_1^{(r)})}{2\pi\beta_2}. \tag{8}$$

The total nonlinear PSDs in spatial mode r in an M-mode FMF are then given by:

$$G_{\text{NLI}}^{(r)} = \sum_{m=1}^{M}\sum_{n=1}^{M}\sum_{p=1}^{M}\eta^{(mnpr)}G^{(m)}G^{(n)}G^{(p)}, \tag{9}$$

where $G^{(m)}$, $G^{(n)}$, and $G^{(p)}$ are, respectively, the PSDs of spatial modes m, n, and p. Only interactions between pairs of spatial modes are considered (i.e., $m = r, n = p$, or $n = r, m = p$), since the other interactions give rise to unstable FWM processes that can be neglected [23]. Under this assumption, Eq. (9) becomes:

$$G_{\text{NLI}}^{(r)} = G^{(r)}\left\{\eta^{(rrrr)}[G^{(r)}]^2 + 2\sum_{n=1,n\neq r}^{M}(\eta^{(rnnr)} + \eta^{(nrrn)})[G^{(r)}]^2\right\} = G^{(r)}\left\{\eta^{(rrrr)}[G^{(r)}]^2 + \sum_{n=1,n\neq r}^{M}(4\eta^{(rnnr)}[G^{(r)}]^2)\right\}. \tag{10}$$

The first term represents the intramodal nonlinear PSD, whereas the second term is the total inter-modal nonlinear PSDs given by the contribution of the interacting spatial modes. The factor of 2 in the first row of the equation is

due to the fact that two polarizations have been considered for each mode. The second row is obtained considering $\eta^{(rnnr)} = \eta^{(nrrn)}$, since we only have interactions between pairs of spatial modes.

The total nonlinear power $P_{\mathrm{NLI}}^{(r)}$ in spatial mode r and the amplified spontaneous emission (ASE) noise power P_{ASE} in the amplifiers are the main sources of degradation of QoT, decreasing the OSNR. Considering an FMF link composed of N_s spans of identical lengths, we obtain:

$$P_{\mathrm{NLI}}^{(r)} \cong N_s G_{\mathrm{NLI}}^{(r)} B_{\mathrm{ref}}, \tag{11}$$

and

$$P_{\mathrm{ASE}} \cong N_s F_n h\nu G B_{\mathrm{ref}} = N_s G_{\mathrm{ASE}} B_{\mathrm{ref}}, \tag{12}$$

where F_n is the noise figure of the amplifiers, $h\nu$ is the photon energy, B_{ref} is the reference noise bandwidth, G is the amplifier gain, and G_{ASE} is the noise PSD in the amplifiers, assumed to be the same for all spatial modes in our model.

Then $\mathrm{OSNR}_{\mathrm{FMF}}^{(r)}$ for spatial mode r in an FMF is [15]:

$$\mathrm{OSNR}_{\mathrm{FMF}}^{(r)} = \frac{P_{\mathrm{ch}}}{N_s (G_{\mathrm{ASE}} + G_{\mathrm{NLI}}^{(r)}) B_{\mathrm{ref}}}, \tag{13}$$

where P_{ch} is the input channel power.

Equation (13) can also describe BuSMFs, considering P_{NLI} only accounts for intramodal nonlinearities.

Current nonlinear models [20,21,27] assume the same input power for all spatial modes, ideal span-by-span optical amplification that perfectly compensates for the loss of the previous span, and spans with equal lengths and same loss coefficients for all spatial modes. In a realistic scenario, however, the overall loss that each spatial mode path experiences is different due to MDLs in the fiber and the multiplexing and switching components, as well as the mode-dependent gain (MDG) of the few-mode erbium-doped fiber amplifiers (FM-EDFAs) [28]. An attempt to account for the impact of MDLs on a networking study has been presented in Ref. [19], based on a model for strongly coupled FMFs [29] without considering nonlinearities. However, in most practical cases, one will be interested in FMF systems with up to six spatial modes, which are mainly considered to operate in the weakly coupled regime (as in the nonlinear models presented in Refs. [20,21,27]). As of today, to the best of our knowledge, no analytical model including the impact of both nonlinearities and MDLs/MDG has been presented so far, due to the increased complexity (and, therefore, impracticability) of such a model. As a result, here we only focus on current analytical nonlinear models that exclude the impact of MDLs/MDG on the system performance [20,21], leaving their inclusion for future studies.

B. Analytical Model for MCFs

The FWM effect due to signals propagating in different cores is defined in a similar way to the case of FMFs. Indeed, considering single-mode cores and three wavelengths λ_1, λ_2, and λ_3 propagating in cores m, n, and p, respectively, a signal is generated at frequency of $\omega_{\lambda_4} = \omega_{\lambda_1} + \omega_{\lambda_2} - \omega_{\lambda_3}$ in core r, with a FWM efficiency given by:

$$\eta^{(mnpr)} = \frac{[\tilde{\gamma}^{(mnpr)}]^2}{\pi\alpha|\beta_2|} \ln\left(\frac{B^2}{2f_w^2}\right), \tag{14}$$

where f_w is the walk-off bandwidth, $\tilde{\gamma}^{2(mnpr)}$ is the nonlinear coefficient, α is the attenuation coefficient, β_2 is the GVD, and B is the overall bandwidth of the channel. Therefore, as is the case for FMFs, the total nonlinear PSDs in core r are:

$$G_{\mathrm{NLI}}^{(r)} = \sum_{m=1}^{C} \sum_{n=1}^{C} \sum_{p=1}^{C} \eta^{(mnpr)} G^{(m)} G^{(n)} G^{(p)}, \tag{15}$$

where $G^{(m)}$, $G^{(n)}$, and $G^{(p)}$ are, respectively, the PSDs in cores m, n, and p, and C is the total number of cores. The above equation can be derived easily by setting the velocity-matched offset, $\Delta f^{(mnpr)}$, to 0 in Eq. (8). This is a valid assumption for MCFs with homogeneous cores with equal mode velocities.

The total nonlinear power $P_{\mathrm{NLI}}^{(r)}$ and ASE noise power P_{ASE} in the amplifiers are also given, respectively, by Eqs. (11) and (12), as in the case of FMFs.

When it comes to estimating the impact on one core of its surrounding cores in an MCF, the fabrication parameters need to be taken into consideration. Depending on the distance between the cores (and, consequently, the number of cores) and other parameters, such as the refractive index profile of each core, MCFs can have strongly coupled or weakly coupled cores. In the former case, a MIMO DSP is required, which will ideally correct all effects of linear crosstalk (XT) between the cores. Conversely, in the latter case, one will lean toward doing away with the MIMO DSP to bring down dispensable expenses, and linear XT will necessarily have to be considered for the evaluation of the OSNR degradation. Therefore, unlike in the FMF case, the OSNR formula will have to factor in the following additional term [30,31]:

$$P_{\mathrm{XT}}^{(r)} \cong N_s \mu_{\mathrm{XT}}^{(r)} P_{\mathrm{ch}}, \tag{16}$$

where N_s is the number of spans and $\mu_{\mathrm{XT}}^{(r)}$ is the XT parameter, given by:

$$\mu_{\mathrm{XT}}^{(r)} \cong \sum_{n=1, n\neq r}^{C} \eta_{\mathrm{coupl}}^{(nr)} L_{\mathrm{span}}, \tag{17}$$

where L_{span} is the span length and $\eta_{\mathrm{coupl}}^{(nr)}$ is the power coupling coefficient between cores n and r [31–33].

In the case of homogeneous MCFs, the previous equation can be simplified as expressed by the following formula:

$$\mu_{\mathrm{XT}}^{(r)} \cong N_c \eta_{\mathrm{coupl}} L_{\mathrm{span}}, \tag{18}$$

where N_c is the number of cores adjacent to core r.

Taking all these terms into account, the OSNR for core r in a homogenous WC-MCF can be written as:

$$\mathrm{OSNR}^{(r)}_{\mathrm{MCF}} = \frac{P_{\mathrm{ch}}}{N_s(G_{\mathrm{ASE}} + G^{(r)}_{\mathrm{NLI}})B_{\mathrm{ref}} + P^{(r)}_{\mathrm{XT}}}. \quad (19)$$

C. Simulation Environment

The QoT estimator is designed to receive as input some parameters providing information about the transceiver model and the transmission channel. The output of the tool produces fundamental metrics in establishing impairment-aware optical connections.

The estimation mechanism requires input parameters to describe the transmitting system, such as input power per channel (P_{ch}), number of co-propagating spectral channels (N_{ch}), number of links (N_{linkss}), number of spans in a link (N_{spans}), span length (L_{span}), symbol rate (R_s), channel spacing (Δf), and modulation format (*ModFormat*). Additional parameters are needed according to the model to be used for the simulations (FMF, MCF, or BuSMF), and also to specify the characteristics of the fiber employed as the transmission channel.

For the FMF case, the QoT estimator requires the closed-form equations, Eqs. (11) and (12), to calculate the total nonlinear interference noise powers $P^{(r)}_{\mathrm{NLI}}$ and P_{ASE}, respectively, for each fiber spatial mode d. For the MCF case, the QoT estimator requires Eqs. (11), (12), and (16) to calculate, respectively, $P^{(r)}_{\mathrm{NLI}}$, P_{ASE}, and the linear XT power $P^{(r)}_{\mathrm{XT}}$ for fiber core r. For the BuSMF case, the same equations apply as for the MCF case, with $P^{(r)}_{\mathrm{XT}} = 0$ and $P^{(r)}_{\mathrm{NLI}}$ only accounting for intramodal contributions. The signal-to-noise ratio (SNR) corresponding to the $\mathrm{OSNR}^{(r)}_{\mathrm{FMF}}$ or $\mathrm{OSNR}^{(r)}_{\mathrm{MCF}}$ value for spatial mode or core d, obtained as reported in Eq. (13) or (19), respectively, can be calculated as [34]:

$$\mathrm{SNR}_{\mathrm{ASE,NLI}} = \frac{\mathrm{OSNR}^{(r)}_{\mathrm{FMF(or\ MCF)}} * B_{\mathrm{ref}}}{N_p * B_{rx}}, \quad (20)$$

where B_{ref} is the reference noise bandwidth, N_p is the number of polarizations, and B_{rx} is the receiver filter bandwidth. The total SNR, in turn, is given by [21]:

$$\mathrm{SNR} = \frac{1}{\frac{1}{\mathrm{SNR}_{XI}} + \frac{1}{\mathrm{SNR}_{\mathrm{ASE,NLI}}}}, \quad (21)$$

where SNR_{XI} is the SNR value accounting for interchannel *XT* (between spectral channels within the same spatial mode) and inter-symbol interference in back-to-back measurements for different modulation formats and spectral widths of the signal [29].

BER values can be calculated from SNR_{XI} for different modulation formats, according to the following formulas [34]:

- for PM-BPSK:

$$\mathrm{BER} = \frac{1}{2}\mathrm{erfc}\left(\sqrt{\mathrm{SNR}}\right), \quad (22)$$

- for PM-QPSK:

$$\mathrm{BER} = \frac{1}{2}\mathrm{erfc}\left(\sqrt{\mathrm{SNR}/2}\right), \quad (23)$$

- for PM-8QAM:

$$\mathrm{BER} = \frac{2}{3}\mathrm{erfc}\left(\sqrt{\frac{3}{14}\mathrm{SNR}}\right), \quad (24)$$

- for PM-16QAM:

$$\mathrm{BER} = \frac{3}{8}\mathrm{erfc}\left(\sqrt{\frac{1}{10}SNR}\right), \quad (25)$$

where $\mathrm{erfc}(x)$ is the complementary error function $\mathrm{erfc}(x) = 2/\sqrt{\pi}\int_x^{\infty} \exp(-t^2)\mathrm{d}t$.

The Q-factor can be computed from the BER as follows:

$$Q = 20\log_{10}\left(\sqrt{2}\mathrm{erfc}^{-1}(2 * \mathrm{BER})\right), \quad (26)$$

where $\mathrm{erfc}^{-1}(x)$ is the inverse of the complementary error function.

D. Transmission Model

The transceiver model considered for the simulations is a WDM superchannel composed of nine co-propagating spectral channels with a symbol rate of $R_s = 32$ GBaud and subcarrier spacings of $\Delta f = 32$ GHz (Nyquist), $\Delta f = 37.5$ GHz, and $\Delta f = 50$ GHz. The simulated transceivers are characterized by four different modulation formats, namely, polarization multiplexed (PM) binary phase shift keying (BPSK), PM-quaternary phase shift keying (PM-QPSK), PM 8 quadrature amplitude modulation (PM-8QAM), and PM 16 quadrature amplitude modulation (PM-16QAM).

The transmission channel is represented by a multispan system with 100 km of FMF or MCF spans. After each fiber span, an EDFA with a noise figure (F_n) of 5 dB completely compensates for the attenuation of the preceding span. These details are summarized in Table I.

In the case of FMF, the reference fiber considered for the simulations is an FMF supporting four non-degenerate LP spatial modes, i.e., a six-mode FMF with spatial modes LP_{01}, $\mathrm{LP}_{11a}/\mathrm{LP}_{11b}$, LP_{02}, and $\mathrm{LP}_{21a}/\mathrm{LP}_{21b}$ [21]. For this fiber, $M = 6$ and the intramodal $\kappa^{(pp)}$ and inter-modal $\kappa^{(mp)}$ averaging factors in Eqs. (2) and (3) are equal to $\frac{16}{11}$ and $\frac{4}{3}$ respectively. Only the interaction between pairs of spatial modes is considered in the model presented in this paper. Therefore, only inter-modal effective area $A^{(mp)}_{\mathrm{eff}}$ values required for the estimation of Eqs. (2) and (3) are presented in the matrix in Table II. Likewise, for the calculation of Eq. (8), Table III shows the relative differential mode delays for all six spatial modes with respect to LP01.

TABLE I
TRANSCEIVER PARAMETERS

N_{ch}	R_s [GBd]	L_{span} [km]	*NF* [dB]	Δf [GHz]
9	32	100	5	32, 37.5, 50

TABLE II
EFFECTIVE AREA [μm^2] OF A SIX-MODE FMF

	LP01	LP02	LP11a	LP11b	LP21a	LP21b
LP01	146	291	291	291	583	583
LP02	291	290	578	578	578	578
LP11a	291	578	193	579	386	386
LP11b	291	578	579	193	386	386
LP21a	583	578	386	386	257	772
LP21b	583	578	386	386	772	257

TABLE III
DIFFERENTIAL MODE DELAY [PS/KM] BETWEEN PAIRS OF MODES OF A SIX-MODE FMF

	LP01	LP02	LP11a	LP11b	LP21a	LP21b
LP01	0	8	13	14	17	18

TABLE IV
FIBER PARAMETERS FOR FMF SIMULATIONS

α [dB/km]	CD [ps/nm/km]	n_2 [m^2/W]	κ_{pp}	κ_{mp}
0.2	20	$2.6 * 10^{-20}$	16/11	4/3

Finally, we assume that all the LP modes are affected by the same amount of chromatic dispersion (CD), i.e., 20 ps/nm/km and the attenuation parameter and nonlinear index are $\alpha = 0.2$ dB/km and $n_2 = 2.6 * 10^{-20}$ m^2/W, respectively. These values are summarized in Table IV.

For the MCF simulations, we assume a seven-core MCF with identical hexagonally arranged pure-silica cores [31]. Since the $P_{XT}^{(d)}$ in each core depends on the contribution of adjacent cores, as shown in Eq. (18), two cases can be distinguished for this fiber configuration:

- XT in the center core, representing the worst-case scenario since the center core has six adjacent cores ($N_c = 6$)
- XT in the outer cores, affected only by the center core and the two adjacent outer cores ($N_c = 3$).

We consider the values of the statistical mean of XT $\mu_{XT}^{(d)}$ at $\lambda = 1550$ nm extracted from Table 2 of Ref. [16]. $\mu_{XT}^{(d)}$ is used to conveniently compute the power coupling coefficient $\eta_{coupl,bd}$. The effective area is fixed to 75 μm^2, CD to 16.7 ps/nm/km, and the nonlinear index (n_2) to $2.3{*}10^{-20} m^2$/W. The attenuation parameter is again set to $\alpha = 0.2$ dB/km. These parameters are presented in Table V.

E. Simulation Results

The SDM QoT estimator allowed for, by a set of simulations, quantitative comparison of the performance of FMFs, MCFs, and BuSMFs, and, thus, evaluation of the impact of the physical impairments. A six-mode FMF, a seven-core WC-MCF, and a bundle of six SMFs were considered, and their performance was compared in terms of maximum optical reach. The fiber parameters used are those reported in Tables IV and V. In order to evaluate the penalty introduced by the use of more complex modulation formats, we consider the four modulation formats described in the previous section. To determine the maximum reach that a Sp-Ch can achieve, we assumed a multispan system with the parameters indicated in Table I and $\Delta f = 50$ GHz. The maximum reach as a function of launch power for the case of nine co-propagating channels per mode/core is depicted in Fig. 1 for the BuSMF, FMF, and WC-MCF.

TABLE V
PARAMETERS FOR MCF SIMULATIONS

α [dB/km]	CD [ps/nm/km]	n_2 [m^2/W]	A_{eff} [μm^2]	$\mu_{XT,d}$ [dB]
0.2	16.7	$2.3 * 10^{-20}$	75	−61.3

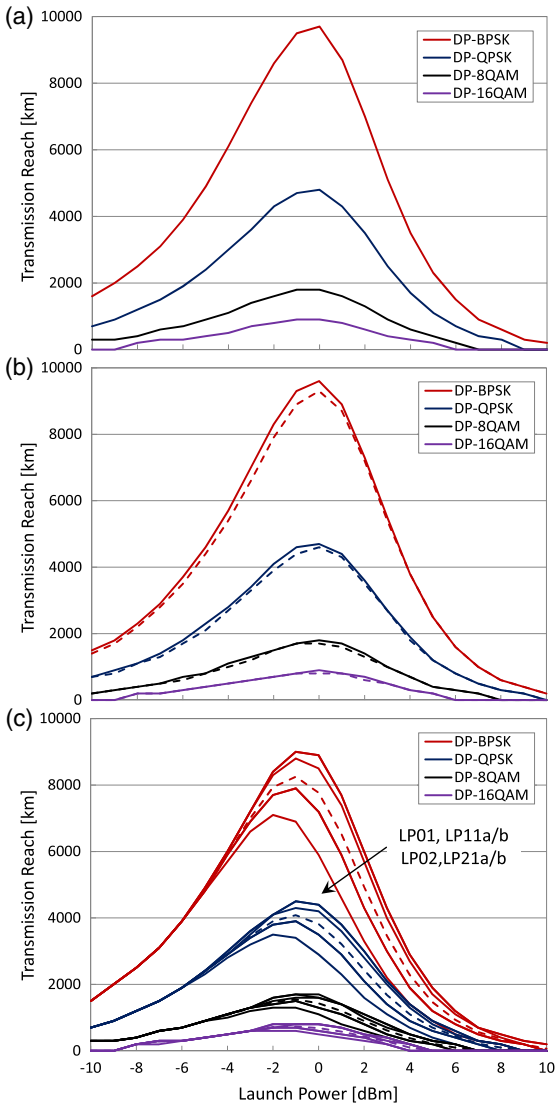

Fig. 1. Maximum reach as a function of launch power for (a) a bundle of SMFs, (b) a seven-core WC-MCF, and (c) a six-mode FMF. In (b), dashed and solid lines indicate, respectively, the results for the outer core and inner core of a seven-core MCF. In (c), solid lines indicate the reach values for different modes from LP01 to LP21a/b, whereas dashed lines indicate the average values.

All fibers in the BuSMF [Fig. 1(a)] showed the same performance due to no interfiber XT. For the MCF case [Fig. 1(b)], the performance of the outer cores (solid lines) is very similar to the case of the BuSMF, whereas the inner core (dashed lines), which is affected by all outer cores, performs slightly worse. Different modes in the FMF show dissimilar performance [Fig. 1(c)], with LP21a/b showing the worst performance. Note that the estimation of transmission reach depends on the span length considered, since the value of the BER is calculated span by span, then the value obtained is compared with the target BER. In addition to span length, the number of co-propagating channels and the channel spacing are two parameters affecting the transmission reach. We performed a set of simulations to determine the impact of these parameters on the achievable reach, and the results are shown in Figs. 2(a)–2(c). For the MCF, the values depicted are referred only to the center core. A mean distance value over the six modes and the worst-case value are considered for the FMF.

Figure 2(a) reports the maximum reach values obtained by varying the span length. The simulations were performed keeping the symbol rate fixed to 32 GBaud, the channel spacing to 50 GHz, and the number of co-propagating channels to 10. Each value is obtained considering the optimal power for that case. The graph shows how the reach decreases when the length of the span increases. Note that, in the MCF case, for higher powers (when the amplification span length is shorter) the linear XT is higher. So it shows poor performance compared with the BuSMF for short spans, whereas it converges to the performance of the BuSMF for long spans. The impact of increase of fiber length on the transmission reach is stronger when less complex modulation formats such as BPSK or QPSK are employed. The picture also shows the maximum reach values that can be achieved in each scenario with a given span length. Figure 2(b) describes the variation of transmission reach when the number of co-propagating channels composing the Sp-Ch is changed. A span length of 100 km is considered for the results shown in Figs. 2(b) and 2(c). The channels considered are spaced apart by 50 GHz. From the graph, it is clear that high-level modulation formats incur a higher OSNR penalty, resulting in a shorter transmission reach, but are more robust to the increase of the number of co-propagating channels since no significant decrease in optical reach was measured.

Finally, Fig. 2(c) shows the effect of channel spacing variation on the maximum optical reach for the optimum launch power. Obviously, an increase of transparent reach is accomplished by increasing the spacing between the subcarriers in the Sp-Ch, even if this results in a higher bandwidth occupancy for the Sp-Ch with a consequent decrease in spectral efficiency.

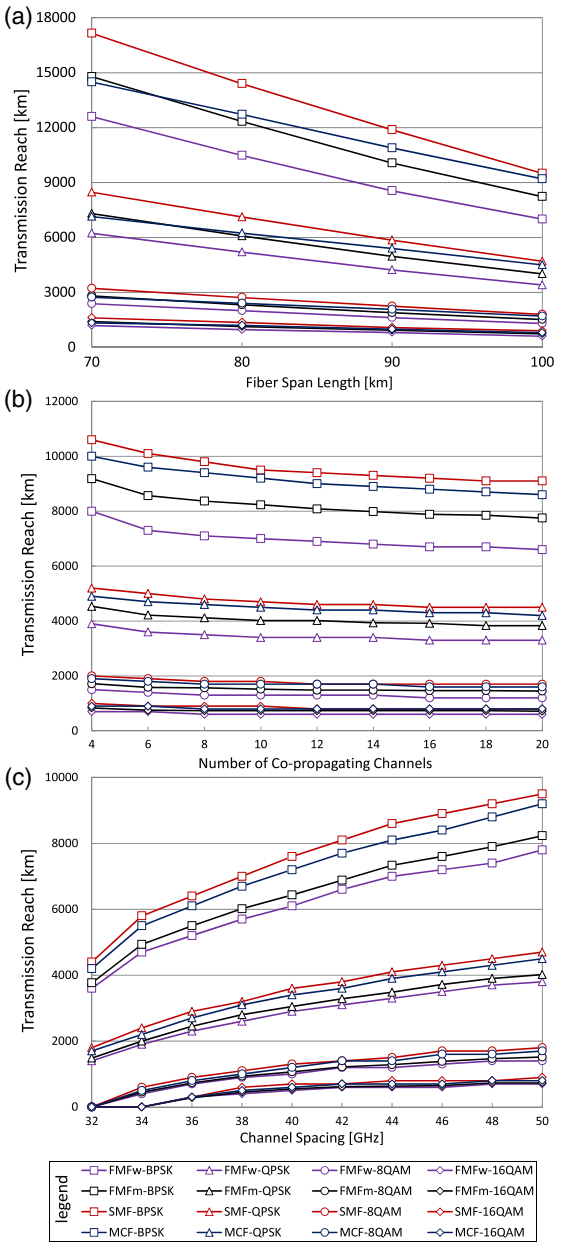

Fig. 2. (a) Maximum reach as a function of fiber span length. (b) Maximum reach as a function of the number of co-propagating channels. (c) Maximum reach as a function of channel spacing.

F. End-to-End QoT Estimator

From a practical point of view, there are multiple active connections in a network, which results in links accommodating a different number of channels from different end-to-end connections. Therefore, for a given lightpath, the signal-related characteristics are not the same for each link. The QoT estimator module is designed to provide a separate estimation for each point-to-point link in between nodes. Then the overall performance of the lightpath is estimated by concatenating the degradation effects from each link in the OSNR values according to [15]. In order to perform a networking-level analysis, we upgrade the offline planning tool proposed in Ref. [9] with the QoT estimator following the LOGON approach [15]. The QoT estimator works in cooperation with other modules of the offline planning tool, and, in particular, with the routing, space, modulation format, and spectrum assignment module, in order to minimize the spectrum utilization and spectrum

fragmentation, while maintaining the required maximum BER. The upgraded offline planning tool thus accounts for physical layer impairments of different types of SDM fibers and the extra constraints imposed by SDM switching technologies.

IV. Network-Wide Performance Evaluation

Selection of a proper transmission medium is one of the key decisions to be made for the development of SDM networks. In principle, a proper option is the one which not only offers good performance, but also imposes a reasonable level of component complexity and deployment cost. This is due to the fact that the complexity of the components (transceiver, switches, amplifiers, etc.) for realizing a particular flavor of SDM network is highly fiber-dependent. Studying the complexity of the components required for SDM networks based on different types of fibers is out of the scope of our work. However, it is of utmost importance to investigate the performance of SDM networks based on the different fiber options pointed out in this paper to showcase the benefits of the developed QoT tool for SDM-based optical network planning practices.

In order to carry out the studies, we consider the topology of the Telefónica Spain national network and its traffic matrix as described in Ref. [12]. In our analysis, we assume two versions of the topology: one with the original link lengths, with an average link length of 135 km, and one where we double the link lengths to evaluate the impact of the geographical size of the network on the performance of SDM networks utilizing alternative transmission media. We should also highlight that, even though there are limitations with the adopted physical layer model, since it just considers the operation in the weak-coupling regime, the distances we are considering in our analysis are indeed possible with proper SDM system configurations, as has been demonstrated in recent works related to transmission experiments using FMFs for long-haul applications [35].

As mentioned in the first paragraph, the choice of a transmission medium is a key factor in determining the required architecture of the optical switches in an SDM-based network. BuSMFs and WC-MCFs are compatible with all SDM switching paradigms described in the introduction [12]; however, it is necessary to consider J-Sw when FMFs are in place, since all the spatial modes of the FMFs have to be switched together and received by the same receiver, allowing the MIMO-based DSP to correctly retrieve the intermixed information across different spatial modes [7].

Therefore, we choose J-Sw as the switching technology for our study, since it is compatible with all SDM fiber options. Note that selecting this option allows us to focus solely on the performance of the transmission media, which is the goal of this study, regardless of the flexibility/constraints imposed by the switching schemes, whose impact is thoroughly investigated in Refs. [9–12,36,37]. Regarding transmission technology, the spatial Sp-Ch allocation scheme is used, which is also compatible with the J-Sw scheme. For the networking study, we consider a six-mode FMF, a bundle of six SMFs, and a seven-core MCF in which we only use the six outer cores to have the same amount of available capacity per link regardless of the fiber type. For the FMF case, two baselines for estimating the QoT are assumed: (1) based on the average (mean) of the QoT values of the six modes, and (2) based on the worst QoT values, i.e., LP21a/b, which are labeled "FMFm" and "FMFw", respectively, in the figures. We consider two metrics for comparison purposes: the average spectrum utilization of the network and the corresponding number of required transceivers operating over different modulation formats. Figure 3 shows the networking-level performance in terms of the average spectrum utilization for the two different sizes of topology under study: (a) the actual sized topology (D) and (b) the doubled sized topology ($2D$). Note that, in this context, performance improvement is achieved when the average spectrum utilization decreases. The performance of networks based on BuSMFs and MCFs is quite similar, even though a slight degradation in the performance of MCF-based networks is observed in the case of the large-scale topology (Fig. 3). This degradation is more evident while looking at the number of required transceivers (TRxs) operating over different modulation formats plotted in Fig. 4. Considering the large-scale topology [Fig. 4(b)], the case utilizing MCFs uses a higher number of less spectrally efficient TRxs (8QAM compared with 16QAM) compared with the one based on SMFs, resulting in a slightly higher number of TRxs for the MCF case. This difference is also shown in Fig. 5(b).

While considering networks utilizing FMFs based on the worst QoT value (FMFw), a significant difference in performance between the SMF and MCF cases is observed. This difference in performance becomes more pronounced for the larger network. This performance difference is well illustrated in Figs. 4 and 5. The FMFw case not only

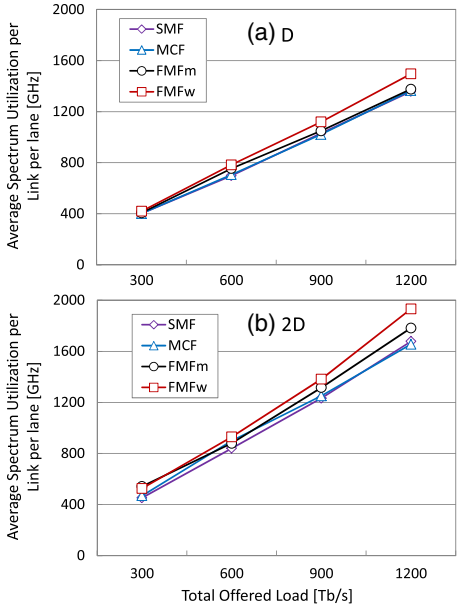

Fig. 3. Average spectrum utilization for (a) the actual sized topology (D) and (b) the doubled sized topology (2D).

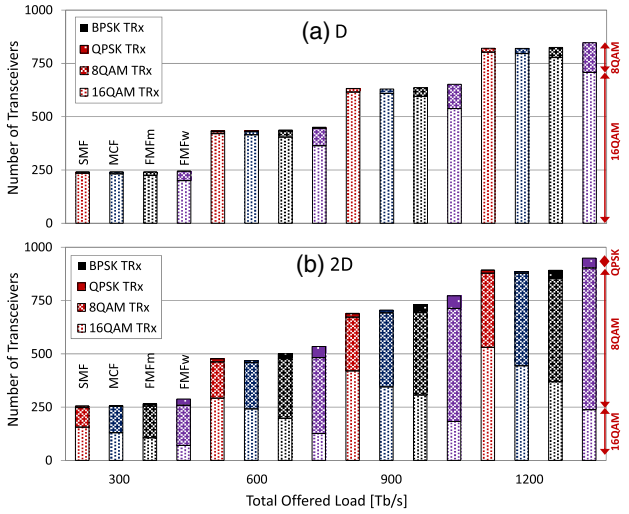

Fig. 4. Number of required transceivers for (a) the actual sized topology (D) and (b) the doubled sized topology (2D).

requires many more TRxs, regardless of the topology size, but also necessitates the use of much lesser spectrally efficient TRxs compared with the other transmission media. In the large-scale topology, it requires 90 more TRxs in total compared with the BuSMF-based network. In addition, out of the total number of in-operation TRxs, only ~24% can operate over the 16QAM format, whereas this approaches 60% for the case of BuSMFs. In other words, by using FMFs instead of SMFs, the number of in-operation TRxs over 16QAM decreases sharply and, instead, more TRxs with lower spectral efficiency are launched, resulting in a higher amount of spectrum utilization in the network.

Considering spatially integrated Sp-Ch TRxs, it is expected that a single common forward error correction (FEC) code is used for all spatial channels, enabling the signals traversing the FMF-based network to travel as far as the average of the reach values of all six modes. Therefore, in order to show the performance benefits of such an option enabled by integrated TRxs, we consider this case in our analysis (labeled FMFm). Under such circumstances, it is observed that the performance of FMF-based networks can be enhanced significantly and approaches the performance of the cases of BuSMFs and MCFs for small-scale topologies. Additionally, for the large topology, it can greatly improve the performance of networks based on FMFs. As shown in Fig. 4, it requires deploying fewer TRxs compared with the FMFw case for the same amount of load offered to the network. In addition, as shown in Fig. 5, the number of TRxs operating over more spectrally efficient modulation formats increases compared with FMFw. However, it still performs quite badly compared with BuSMFs and WC-MCFs for large-scale topologies. Therefore, even though the introduction of a common FEC code may enhance the performance of FMF-based SDM networks and make them favorable for small-scale topologies, they lack enough potential to be considered for large-scale topologies. Regardless of their performance, the complexity of DSP and its corresponding power consumption may be a showstopper for FMF-based SDM networks. On the other hand, other components used for networks based on FMFs, like integrated amplifiers (e.g., FM-EDFAs) and switching nodes, can reduce power consumption [5]. Note that, while the DSP complexity in the case of BuSMFs and WC-MCFs is similar to that of conventional SMF-based systems, it is higher for the FMF cases because of the severe effects of DGD, which in turn results in higher cost and power consumption of the transceivers [14].

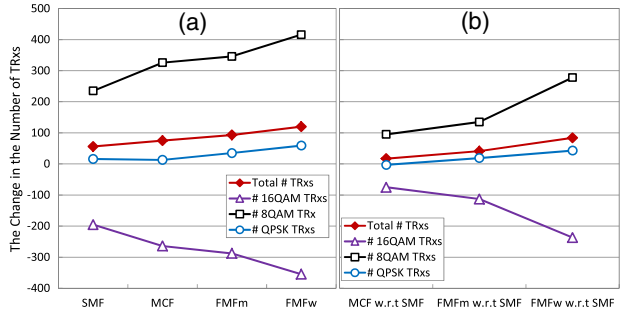

Fig. 5. Change in the number of TRxs (a) while considering the large-scale topology compared with the small one for every fiber type independently, and (b) while considering MCFs/FMFs compared with SMFs for the large-scale topology. Every point in (b) is obtained by subtracting the number of required TRxs for the BuSMF case from the target case. The total offered load is 900 Tb/s.

V. Conclusion

A QoT estimator has been developed using accurate, yet low computationally complex, analytical models for SDM networks. Based on this estimator, the performance of SDM networks using different transmission media has been compared. Considering small-scale topologies, FMF-based SDM networks show slightly worse performance compared with the case of BuSMFs and WC-MCFs. However, for large-scale topologies, SDM networks based on BuSMFs and MCFs show significantly better performance, mainly in terms of the amount of utilized spectral and spatial resources, which allows the network to support more traffic compared to FMF-based realizations.

It is concluded that FMFs can be an option to be considered for small-scale networks, even though it requires a more complex MIMO DSP, which translates into higher implementation cost and power consumption. However, for large-scale networks, BuSMFs and MCFs are shown to be the most favorable options for large-scale topologies.

Additionally, the utilization of the already installed SMFs is likely to be the most cost-effective option for near-term realizations of SDM networks. However, in practice, the splicing of BuSMFs with a large number of fibers and their alignment with the TRx is a challenge since it makes the interfacing more difficult and costly compared with the FMF case. MCFs also pose the same problem. On the other hand, MCFs and FMFs offer reduced-size cables with higher density and lower weight than BuSMFs.

Acknowledgment

This work was partially supported by the EC through the INSPACE (n. 619732) project and by the Catalan Institution for Research and Advanced Studies (ICREA).

References

[1] E. Agrell, M. Karlsson, A. R. Chraplyvy, D. J. Richardson, P. M. Krummrich, P. Winzer, K. Roberts, J. K. Fischer, S. J. Savory, B. J. Eggleton, M. Secondini, F. R. Kschischang, A. Lord, J. Prat, I. Tomkos, J. E. Bowers, S. Srinivasan, M. Brandt-Pearce, and N. Gisin, "Roadmap of optical communications," *J. Opt.*, vol. 18, no. 6, 063002, 2016.

[2] B. Shariati, D. Klonidis, I. Tomkos, D. M. Marom, M. Blau, S. Ben-Ezra, M. Gerola, D. Siracusa, J. Macdonald, N. Psaila, C. Sanchez-Costa, A. D. Ellis, J. F. Ferran, and F. Jimenez, "Realizing spectrally-spatially flexible optical networks," *IEEE Photon. Soc. Newslett.*, vol. 32, no. 6, pp. 4–9, Dec. 2017.

[3] M. Klinkowski, P. Lechowicz, and K. Walkowiak, "Survey of resource allocation schemes and algorithms in spectrally-spatially flexible optical networking," *J. Opt. Switching Netw.*, vol. 27, pp. 58–78, Jan. 2018.

[4] D. Klonidis, F. Cugini, O. Gerstel, M. Jinno, V. Lopez, E. Palkopoulou, M. Sekiya, D. Siracusa, G. Thouénon, and C. Betoule, "Spectrally and spatially flexible optical network planning and operations," *IEEE Commun. Mag.*, vol. 53, no. 2, pp. 69–78, Feb. 2015.

[5] J. M. Rivas-Moscoso, B. Shariati, A. Mastropaolo, D. Klonidis, and I. Tomkos, "Cost benefit quantification of SDM network implementations based on spatially integrated network elements," in *European Conf. on Optical Communication (ECOC)*, 2016, paper M.1.F.4.

[6] D. Richardson, "New optical fibres for high-capacity optical communications," *Philos. Trans. A Math. Phys. Eng. Sci.*, vol. 374, no. 2062, 20140441, Mar. 2016.

[7] D. M. Marom and M. Blau, "Switching solutions for WDM-SDM optical networks," *IEEE Commun. Mag.*, vol. 53, no. 2, pp. 60–68, Feb. 2015.

[8] D. M. Marom, P. D. Colbourne, A. D'errico, N. K. Fontaine, Y. Ikuma, R. Proietti, L. Zong, J. M. Rivas-Moscoso, and I. Tomkos, "Survey of photonic switching architectures and technologies in support of spatially and spectrally flexible optical networking [Invited]," *J. Opt. Commun. Netw.*, vol. 9, no. 1, pp. 1–26, Jan. 2017.

[9] B. Shariati, P. S. Khodashenas, J. M. Rivas-Moscoso, S. Ben-Ezra, D. Klonidis, F. Jiménez, L. Velasco, and I. Tomkos, "Evaluation of the impact of different SDM switching strategies in a network planning scenario," in *Optical Fiber Communication Conf. and Exhibition*, Anaheim, California, Mar. 2016, paper Tu2 H.4.

[10] P. S. Khodasenas, J. M. Rivas-Moscoso, D. Siracusa, F. Pederzolli, B. Shariati, D. Klonidis, E. Salvadori, and I. Tomkos, "Comparison of spectral and spatial super-channel allocation schemes for SDM networks," *J. Lightwave Technol.*, vol. 34, no. 11, pp. 2710–2716, June 2016.

[11] B. Shariati, D. Klonidis, D. Siracusa, F. Pederzolli, J. M. Rivas-Moscoso, L. Velasco, and I. Tomkos, "Impact of traffic profile on the performance of spatial superchannel switching in SDM networks," in *European Conf. on Optical Communication (ECOC)*, 2016, paper M.1.F.1.

[12] B. Shariati, J. M. Rivas-Moscoso, D. M. Marom, S. Ben-Ezra, D. Klonidis, L. Velasco, and I. Tomkos, "Impact of spatial and spectral granularity on the performance of SDM networks based on spatial superchannel switching," *J. Lightwave Technol.*, vol. 35, no. 13, pp. 2559–2568, 2017.

[13] S. O. Arik, J. M. Kahn, and K.-P. Ho, "MIMO signal processing for mode-division multiplexing," *IEEE Signal Process. Mag.*, vol. 31, no. 2, pp. 25–34, Mar. 2014.

[14] N. P. Diamantopoulos, B. Shariati, and I. Tomkos, "On the power consumption of MIMO processing and its impact on the performance of SDM networks," in *Optical Fiber Communication Conf. Exhibition*, Los Angeles, California, 2015, paper Th2 A.18.

[15] P. Poggiolini, G. Bosco, A. Carena, V. Curri, Y. Jiang, and F. Forghieri, "The GN-model of fiber nonlinear propagation and its applications," *J. Lightwave Technol.*, vol. 32, no. 4, pp. 694–721, 2014.

[16] A. Muhammad, G. Zervas, and R. Forchheimer, "Resource allocation for space division multiplexing: optical white box vs. optical black box networking," *J. Lightwave Technol.*, vol. 33, no. 23, pp. 4928–4941, 2015.

[17] M. Dharmaweera, L. Yan, M. Karlsson, and E. Agrell, "Nonlinear-impairments- and crosstalk-aware resource allocation schemes for multicore-fiber-based flexgrid networks," in *European Conf. on Optical Communication (ECOC)*, 2016, paper Th.2.P2.SC6.69.

[18] C. Rottondi, P. Boffi, P. Martelli, and M. Tornatore, "On the benefits of few-mode transmission in ring metro optical networks with flexible grid," in *Optical Fiber Communication Conf. (OFC)*, 2016, paper Tu2H.6.

[19] H. Huang, S. Huang, S. Yin, M. Zhang, J. Zhang, and W. GuH, "Virtual network provisioning over space division multiplexed optical networks using few-mode fibers," *J. Opt. Commun. Netw.*, vol. 8, no. 10, pp. 726–733, 2016.

[20] A. Ellis, N. Mac Suibhne, F. G. Gunning, and S. Sygletos, "Expressions for the nonlinear transmission performance of multi-mode optical fiber," *Opt. Express*, vol. 21, no. 19, pp. 22834–22846, 2013.

[21] F. Ferreira, N. Mac Suibhne, C. Sánchez, S. Sygletos, and A. D. Ellis, "Advantages of strong mode coupling for suppression of nonlinear distortion in few-mode fibers," in *Optical Fiber Communication Conf. (OFC)*, 2016, paper Tu2E.3.

[22] S. Mumtaz, R.-J. Essiambre, and G. P. Agrawal, "Nonlinear propagation in multimode and multicore fibers: generalization of the Manakov equations," *J. Lightwave Technol.*, vol. 31, no. 3, pp. 398–406, 2013.

[23] G. Rademacher and K. Petermann, "Nonlinear Gaussian noise model for multimode fibers with space-division multiplexing," *J. Lightwave Technol.*, vol. 34, no. 9, pp. 2280–2287, 2016.

[24] K. P. Ho and J. M. Kahn, "Linear propagation effects in MDE-division multiplexing systems," *J. Lightwave Technol.*, vol. 32, no. 4, pp. 614–628, Feb. 2014.

[25] P. Sillard, "Scalability of few-mode BERS for mode-division-multiplexed systems," in *IEEE Photonics Conf.*, San Diego, California, 2014, pp. 520–521.

[26] C. Antonelli, M. Shtaif, and A. Mecozzi, "Modeling of nonlinear propagation in space-division multiplexed fiber-optic transmission," *J. Lightwave Technol.*, vol. 34, no. 1, pp. 36–54, Jan. 2016.

[27] G. Rademacher, F. Schmidt, and K. Petermann, "Optimum capacity utilization in space division multiplexed transmission systems with multimode fibers," in *European Conf. on Optical Communication (ECOC)*, 2016, paper Th.2.P2.SC5.62.

[28] N. Bai, E. Ip, T. Wang, and G. Li, "Multimode fiber amplifier with tunable modal gain using a reconfigurable multimode pump," *Opt. Express*, vol. 19, no. 17, pp. 16601–16611, 2011.

[29] K.-P. Ho, "Exact model for mode-dependent gains and losses in multimode fiber," *J. Lightwave Technol.*, vol. 30, pp. 3603–3609, 2012.

[30] X. Chen and W. Shieh, "Closed-form expressions for nonlinear transmission performance of densely spaced coherent optical OFDM systems," *Opt. Express*, vol. 18, no. 18, pp. 19039–19054, 2010.

[31] T. Hayashi, T. Taru, O. Shimakawa, T. Sasaki, and E. Sasaoka, "Uncoupled multi-core fiber enhancing signal-to-noise ratio," *Opt. Express*, vol. 20, no. 26, pp. B94–B103, Dec. 2012.

[32] M. Koshiba, K. Saitoh, K. Takenaga, and S. Matsuo, "Analytical expression of average power-coupling coefficients for estimating intercore crosstalk in multicore fibers," *IEEE Photon. J.*, vol. 4, no. 5, pp. 1987–1995, Oct. 2012.

[33] F. Ye, J. Tu, K. Saitoh, and T. Morioka, "Simple analytical expression for crosstalk estimation in homogeneous trench-assisted multi-core fibers," *Opt. Express*, vol. 22, no. 19, pp. 23007–23018, Sept. 2014.

[34] A. Carena, V. Curri, G. Bosco, P. Poggiolini, and F. Forghieri, "Modeling of the impact of nonlinear propagation effects in uncompensated optical coherent transmission links," *J. Lightwave Technol.*, vol. 30, no. 10, pp. 1524–1539, May 2012.

[35] G. Rademacher, R. Ryf, N. K. Fontaine, H. Chen, R. J. Essiambre, B. J. Puttnam, R. S. Luís, Y. Awaji, N. Wada, S. Gross, N. Riesen, M. Withford, Y. Sun, and R. Lingle, "Long-haul transmission over few-mode fibers with space-division multiplexing," *J. Lightwave Technol.*, vol. 36, no. 6, pp. 1382–1388, 2018.

[36] F. Pederzolli, D. Siracusa, B. Shariati, J. M. Rivas-Moscoso, E. Salvadori, and I. Tomkos, "Improving performance of spatially joint-switched space division multiplexing optical networks via spatial group sharing," *J. Opt. Commun. Netw.*, vol. 9, no. 3, pp. B1–B10, 2017.

[37] J. M. Rivas-Moscoso, B. Shariati, D. M. Marom, D. Klonidis, and I. Tomkos, "Comparison of CD(C) ROADM architectures for space division multiplexed networks," in *Optical Fiber Communication Conf. Exhibition*, Los Angeles, California, 2015, paper Th2A.45.